Astronomy
&
Astrophysics

Near infrared photometric and optical spectroscopic study of 22 low mass star clusters embedded in nebulae[⋆]

J. B. Soares[1,2], E. Bica[1], A. V. Ahumada[3], and J. J. Clariá[3]

[1] Universidade Federal do Rio Grande do Sul, IF, CP 15051, Porto Alegre 91501–970, RS, Brazil
e-mail: jules@if.ufrgs.br
[2] LATO-DCET-UESC, Rodovia Ilhéus-Itabuna, km 16, Ilhéus 45662-000, BA, Brazil
[3] Observatorio Astronómico de Córdoba, Universidad Nacional de Córdoba, Laprida 854, 5000 Córdoba, Argentina

ABSTRACT

Aims. Among the star clusters in the Galaxy, those embedded in nebulae represent the youngest group, which has only recently been explored. The analysis of a sample of 22 candidate embedded stellar systems in reflection nebulae and/or HII environments is presented.
Methods. We employed optical spectroscopic observations of stars in the directions of the clusters carried out at CASLEO (Argentina) together with near infrared photometry from the 2MASS catalogue. Our analysis is based on source surface density, colour–colour diagrams and on theoretical pre-main sequence isochrones. We take into account the field star contamination by carrying out a statistical subtraction.
Results. The studied objects have the characteristics of low mass systems. We derive their fundamental parameters. Most of the cluster ages are younger than 2 Myr. The studied embedded stellar systems in reflection nebulae and/or HII region complexes do not have stars of spectral types earlier than B. The total stellar masses locked in the clusters are in the range $20-220$ $M_\odot$. They are found to be gravitationally unstable and are expected to dissolve in a timescale of a few Myr.

Key words. Galaxy: open clusters and associations: general

1. Introduction

Apart from globular and open clusters in the Galaxy, a new class of star clusters has been detected in recent decades thanks to the development of infrared detectors (see Lada & Lada 2003, for a review). They are the clusters embedded in nebulae, which are in general stellar systems newly formed in giant molecular clouds and associated with emission and/or reflection nebulae. Bica et al. (2003a) provided a catalogue of 276 embedded clusters and stellar groups. The 2MASS database (Skrutskie et al. 2006, and references therein) allowed the discovery of many new embedded clusters (e.g. Ivanov et al. 2002; Dutra et al. 2003; Bica et al. 2003b).

Total masses of embedded clusters within 2 kpc occur mostly in the range of 20 to 1000 $M_\odot$; however, the efforts to study them have been mainly concentrated on those with intermediate and higher total masses (Lada & Lada 2003). On the other hand, lower mass embedded clusters are interesting because they may contain non-ionizing stars as their most massive members, thus producing particular interactions with the interstellar medium (Soares & Bica 2002, 2003; Soares 2006). Optical stars were spectroscopically observed in Soares et al. (2005) aiming at studying the more massive possible members.

The goal of the present work is to carry out a photometric analysis in the near infrared of the stellar content of a sample of 22 low mass cluster candidates (Dutra et al. 2003) from the

2MASS catalogue. We also determine spectral types for possible optical members by using spectroscopic observations carried out at Complejo Astronómico El Leoncito (CASLEO, Argentina). In Sect. 2 we present the selected sample of low mass cluster candidates. In Sect. 3 we provide the photometric and spectroscopic data and in Sect. 4 we describe the methods used. The cluster properties are analysed in Sect. 5 and the concluding remarks are presented in Sect. 6.

2. The embedded star cluster sample

The selected sample of 22 embedded clusters and stellar groups (Table 1) has been taken from Dutra et al. (2003). This sample is not too densely populated and they are all embedded in nebulae (see Sect. 5.2 and Table 1).

Due to the limited resolution of the 2MASS catalogue, we excluded the objects with known distances of the nebulae larger than 2.4 kpc as well as those presenting high stellar density. We illustrate in Fig. 1, DBSB 002 in the HII region Gum 5 and DBSB 011 in the nebula Bran 22C. This figure provides typical IR images for two objects of the current sample.

Table 1 shows the physical and structural parameters for the objects in the selected sample. The columns indicate: (1) object identification; (2) and (3) equatorial coordinates (J2000); (4) related nebula; (5) nebula environment – HII region (HII) or reflection nebula (RN); (6) known distance of the nebula; (7) derived cluster angular radius in arcmin; (8) richness index (Sect. 4); (9) A_J mean absorption; (10) K_s excess fraction (f_{K_s}); (11) total mass.

Table 1. Structural and physical parameters for the clusters and related nebulae.

Cluster	α(J2000)	δ(J2000)	Nebulae	environment	$d_\odot$[kpc]	$r_a{}^a$	Ic^b	$A_J{}^c$	f_{K_s}	$M[M_\odot]$
DBSB 002	07 10 12	−18 26 21	Gum 5	HII	−	1.0	28	1.70 ± 0.08	0.19	−
DBSB 011[†]	07 24 16	−24 38 01	Bran 22C	−	−	2.0	84	1.18 ± 0.07	0.33	−
DBSB 014	07 37 46	−32 50 29	Bran 58	−	−	1.6	38	1.97 ± 0.10	0.29	−
DBSB 030	09 01 54	−44 43 32	Bran 221	−	−	0.6	9	2.23 ± 0.16	−	−
DBSB 031	08 52 30	−48 45 57	vdBH-RN 22a	RN	1.7	1.4	36	1.91 ± 0.12	0.30	67
DBSB 035	09 15 11	−47 28 32	Bran 242	−	−	2.0	52	1.07 ± 0.12	0.25	−
DBSB 039	09 24 25	−53 08 08	Bran 262	−	−	0.6	10	0.74 ± 0.14	−	−
DBSB 040	10 01 22	−57 43 10	Bran 280	RN	−	1.6	41	1.23 ± 0.11	0.31	−
DBSB 041	10 01 28	−57 43 49	Bran 280	RN	−	1.2	28	1.63 ± 0.15	0.45	−
DBSB 042	10 07 33	−57 33 30	Bran 288, RCW 46	HII	−	0.6	11	1.06 ± 0.19	−	−
DBSB 049	10 51 08	−54 20 45	Brana 322B	−	−	2.0	57	0.99 ± 0.10	0.21	−
DBSB 064	11 24 41	−58 56 29	vdBH-RN 48	RN	1.5	0.6	19	0.86 ± 0.10	0.11	35
DBSB 069	11 33 54	−63 16 46	Bran 66, RCW 62	HII	1.7	1.0	20	0.68 ± 0.10	0.18	31
DBSB 070	11 48 36	−62 17 16	Bran 373	HII	1.7	1.0	16	0.86 ± 0.19	0.11	31
DBSB 081	12 58 40	−66 21 05	vdBH-RN 58	RN	1.7	1.0	22	0.45 ± 0.11	−	−
DBSB 087	13 32 47	−60 26 54	ESO 132EN 12	HII	−	0.6	14	2.18 ± 0.45	−	−
DBSB 088[‡]	14 19 40	−61 25 20	RCW 85	HII	1.2	1.2	14	2.73 ± 0.53	0.22	20
DBSB 104	17 04 02	−51 04 55	vdBH-RN 81	RN	−	2.0	35	0.48 ± 0.04	0.11	−
DBSB 109	16 47 11	−41 16 28	vdBH-RN 73a	RN	1.9	1.6	42	1.28 ± 0.12	0.07	120
DBSB 114	16 59 10	−40 12 05	G 345.3+1.5	HII	1.9	1.2	65	1.72 ± 0.08	0.18	219
DBSB 121	17 17 01	−36 22 10	RCW 126	HII	1.4	1.6	42	2.41 ± 0.25	0.50	78
DBSB 123	17 17 15	−36 20 18	RCW 126	HII	1.4	1.6	54	2.61 ± 0.21	0.20	130

[a] Cluster limiting angular radius (arcmin); [b] richness indicator index; [c] A_J mean absorption.

[†] Same as IBP 6 (Ivanov et al. 2002).

[‡] In Dutra et al. (2003) the declination is incorrect but the related nebula is correct. This cluster is the same as GLIMPSE-50 (Mercer et al. 2005).
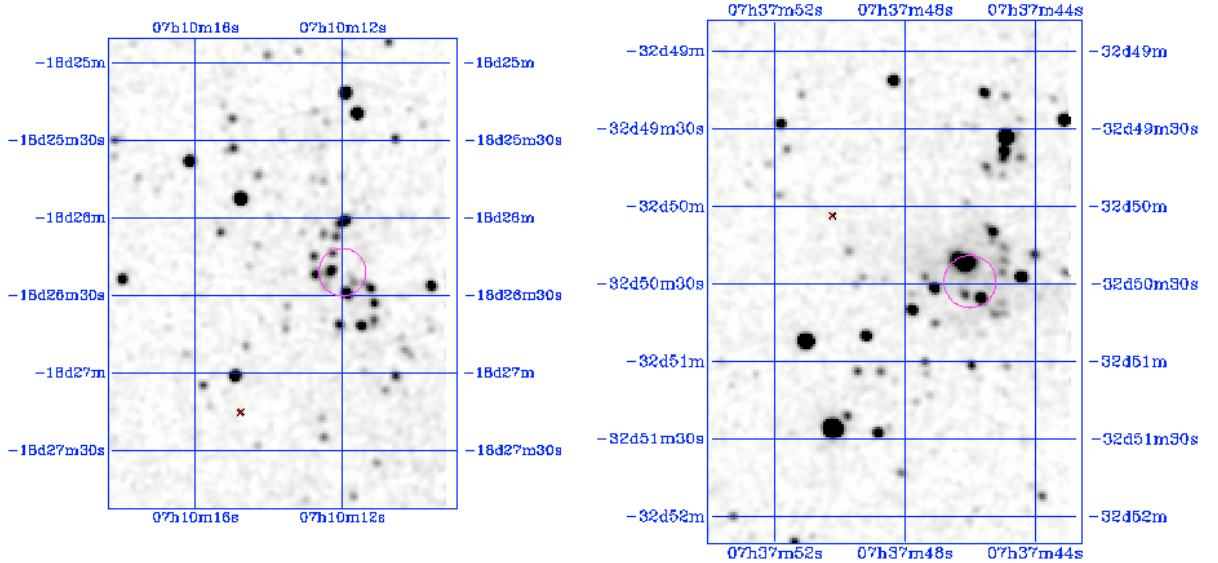
Fig. 1. 2MASS K_s band images of DBSB 002 (*left*) and DBSB 011 (*right*) showing clustering. The small open circle indicates the object's central part.

Object identification and further information about the nebulae shown in Table 1 come from several studies: RCW (Rodgers et al. 1960), Gum (Gum 1955), Bran (Brand et al. 1986), ESO (Lauberts 1982) and G (Caswell & Haynes 1987; Kuchar e Clark 1997). The columns dealing with the cluster parameters are discussed in Sect. 5.

3. Photometric and spectroscopic data

The photometric data were taken from the Two Micron All Sky Survey (2MASS). We employed the Gator tool for Point Source

Catalog extractions, as given in the 2MASS site[1]. An extraction table gives for each star, the J, H and K_s magnitudes, the three corresponding colours ($J − H$, $H − K_s$ and $J − K_s$), the respective errors and the J2000.0 coordinates. The 2MASS photometric errors in the present regions for each magnitude are basically the same as those presented in Soares & Bica (2002) for the regions of NGC 2327 and BRC 27. The errors become large (0.1 mag or larger) for magnitudes fainter than $J = 15.7$, $H = 15$ or $K_s = 14$. For comparison purposes we made extractions up to a radius $r = 5'$ around the object center.

---

[1] http://www.ipac.caltech.edu/2mass
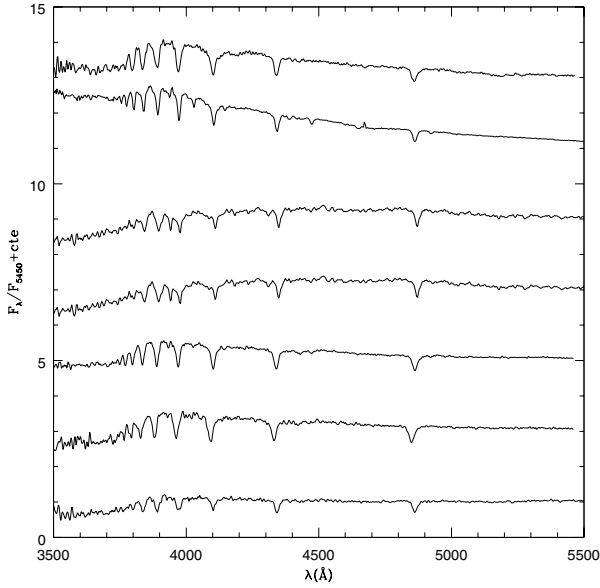
Fig. 2. Observed spectra of the stars in Table 2. *From top to bottom*: DBSB031_1, DBSB039_1, DBSB039_2, DBSB042_1, DBSB049_1, DBSB049_2 and DBSB069_1. Spectra are normalised to $F_\lambda = 1$ at $\lambda = 5450$ Å. Constants have been added to the spectra, except for the bottom one.

The spectroscopic observations were carried out with the Jorge Sahade 2.15 m telescope at CASLEO (Argentina) over 11 nights between October 2005 and April 2006. In all observing runs, we employed a CCD camera containing a Tektronix chip of 1024×1024 pixels attached to a REOSC spectrograph (simple mode), the size of each pixel being $24 \mu \times 24 \mu$. The total field along the slit was $4.7'$, with the slit oriented in the east-west direction. We obtained spectra ranging from 3500 Å to 5600 Å, using a grating of 300 lines/mm. The average dispersion was 140 Å/mm. Three exposures of 20 min were generally taken for each object. Standard stars LTT 1020, LTT 2415, LTT 2511, LTT 3864, LTT 7987 and LTT 9239 (Stone & Baldwin 1983) were used for calibration of the observed spectra. For instrumental calibration purposes, frames of Cu-Ar-Ne comparison lamps were taken between and after the object observations, as well as bias, dome, twilight sky and tungsten lamp flat-fields. The spectra were reduced using the IRAF package. The description of reduction procedures can be seen in Ahumada et al. (2000). The observed spectra are shown in Figs. 2 and 3. The continuum distributions indicate various amounts of reddening.

4. Methods of analysis

We obtained spectral types for the brightest star(s) in each object by means of the template matching method, namely, by achieving the best possible match between the continuum and lines of the analysed star spectrum and the stars in the spectral library of Silva & Cornell (1992).

The analysis method is the same as that used by Ahumada et al. (2001). For the sake of illustrating the method, we show in Fig. 4 the observed spectrum of the star DBSB 049_3, its dereddened spectrum and a B6V template spectrum. From such comparisons, we derived spectral types and reddening values (Table 2).

The source density profile is useful when studying the angular size of star clusters and their number of stellar sources. The angular radius for each star cluster is obtained by considering
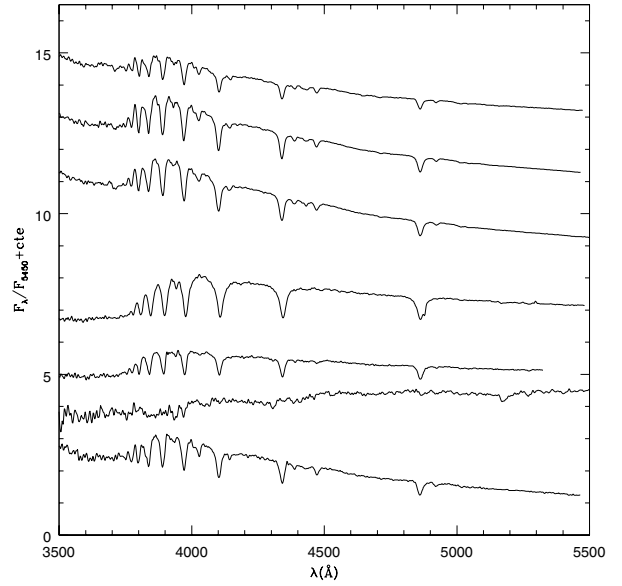

Fig. 3. Same as in Fig. 2 for the remaining stars. *From top to bottom*: DBSB069_2, DBSB070_1, DBSB081_1, DBSB088_1, DBSB104_1, DBSB104_2 and DBSB109_1.
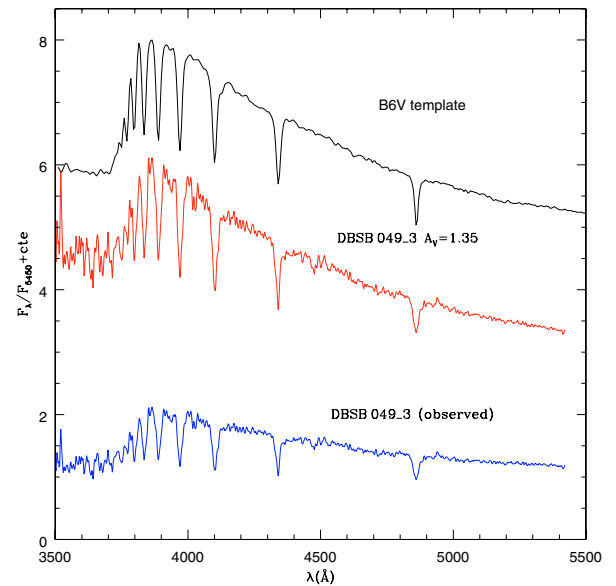
Fig. 4. Observed spectrum of the DBSB 049_3 star, the same spectrum corrected of reddening and the B6V template spectrum (Silva & Cornell 1992). The spectra are normalised at $\lambda = 5450$ Å and shifted by arbitrary constants for comparison purposes, except for the bottom one.

the mean value of the source density profile of the surrounding stellar field.

The number of star cluster members is estimated using the Ic index, i.e., considering the ratio between the number of sources in the direction of the star cluster and that of the surrounding stellar field (Testi et al. 1998). We extracted stars within $5'$ of the assumed center of each object (Table 1), using the 2MASS photometry. By dividing this area into concentric $0.2'$ wide rings, we calculated the number of stars confined within each ring per unit area. The Ic index does not take into account differential extinction. The young cluster regions are expected to present larger extinctions than those of their
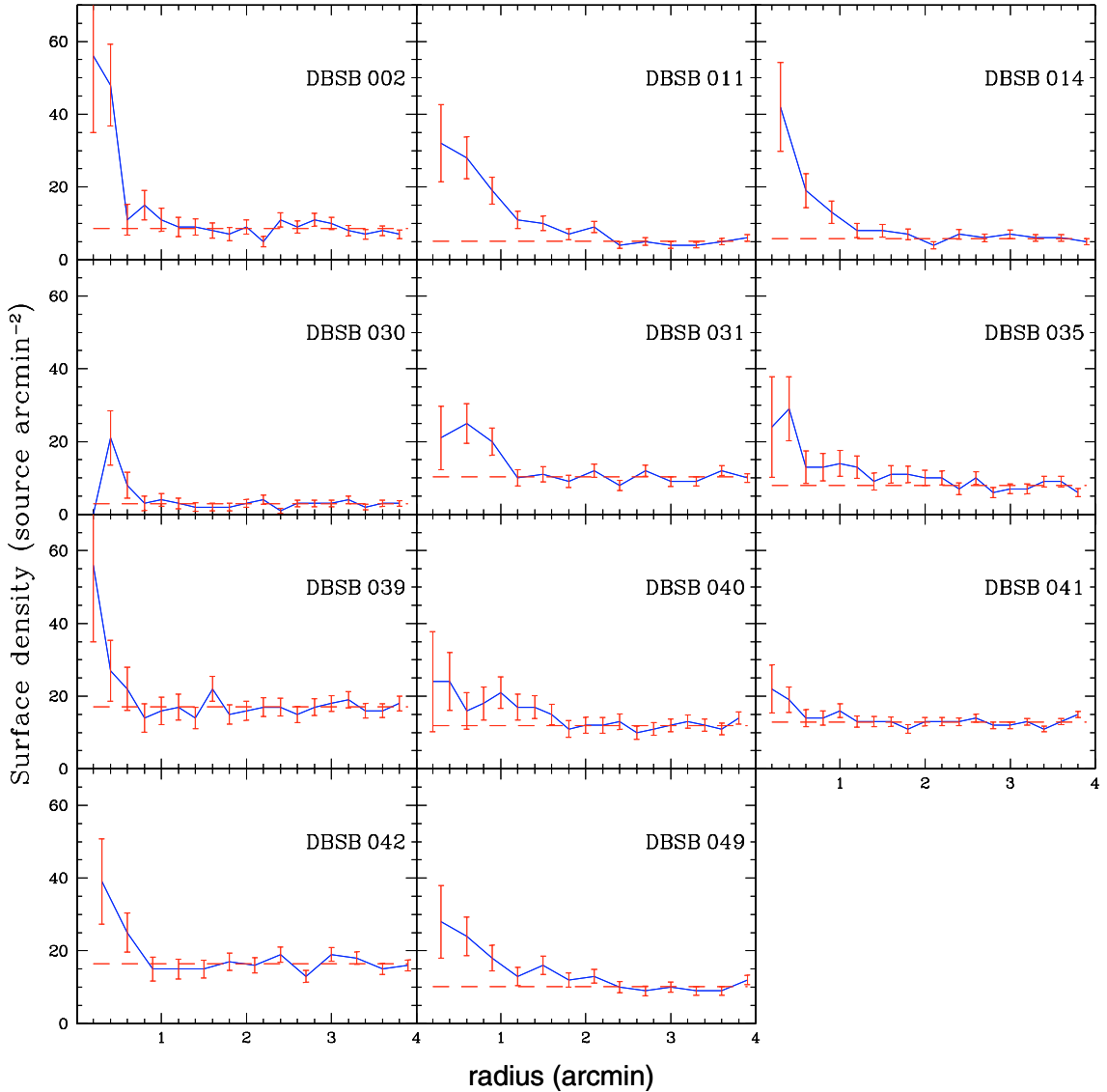
Fig. 5. Source surface density distributions for the studied embedded clusters or stellar groups. The dashed lines indicate the mean background surface density for each object. Poisson errors are indicated.

surroundings. Considering this expected effect, the Ic index could overestimate the observed field star contamination in the cluster regions, resulting in an underestimation of cluster members.

The stellar field was removed from each star cluster by means of a statistical method. The comparisons of the distribution of stars in the colour−colour diagram (2CD) for on-cluster and off-cluster stars are the essence of this statistical field subtraction method. This associates a membership probability (P_{jon}) with each star in the on-cluster area. Details are given in Soares et al. (2005). The 2CD analysis allows us to derive the mean extinction of the embedded clusters, using reddening vectors and intrinsic colours as in Soares et al. (2005). In addition, the 2CD analysis provides information about the evolutionary stage of the cluster, through the fraction of stars with K_s band excess, which is characteristic of pre-main sequence (PMS) stars (Carpenter et al. 1993; Lada & Adams 1992).

The estimated mass for each star cluster was obtained by means of a method similar to that of Lada & Lada (2003). We adopted a universal initial mass function (IMF) for all the

clusters, using the Trapezium cluster IMF derived by Muench et al. (2002) in a study of the luminosity function in the K_s band.

$$\frac{dN}{dm} = M^\alpha \begin{cases} \alpha = -2.21, \ M > 0.600 \ M_\odot \\ \alpha = -1.15, \ 0.600 \ M_\odot < M < 0.120 \ M_\odot \\ \alpha = -0.27, \ 0.120 \ M_\odot < M < 0.025 \ M_\odot \\ \alpha = -6.00, \ 0.025 \ M_\odot < M < 0.017 \ M_\odot. \end{cases}$$

The stellar mass of the faintest detected star in each cluster was obtained considering the detection limit, the distance and the mean extinction for each cluster. The derived mass for the clusters depends on their evolutionary stage. Therefore, isochrones of different ages were used in this analysis.

To derive the total mass for each cluster, we estimated the total number of stars first considering the number of detected stars and the IMF of the Trapezium cluster. We used the following relation between the total mass (M_T) and the total number of stars (N_T) derived for the Trapezium, $M_T/N_T = 0.53$ (Muench et al. 2002).

The cluster age can be estimated by means of the K_s excess method (Soares et al. 2005, and references therein). In this
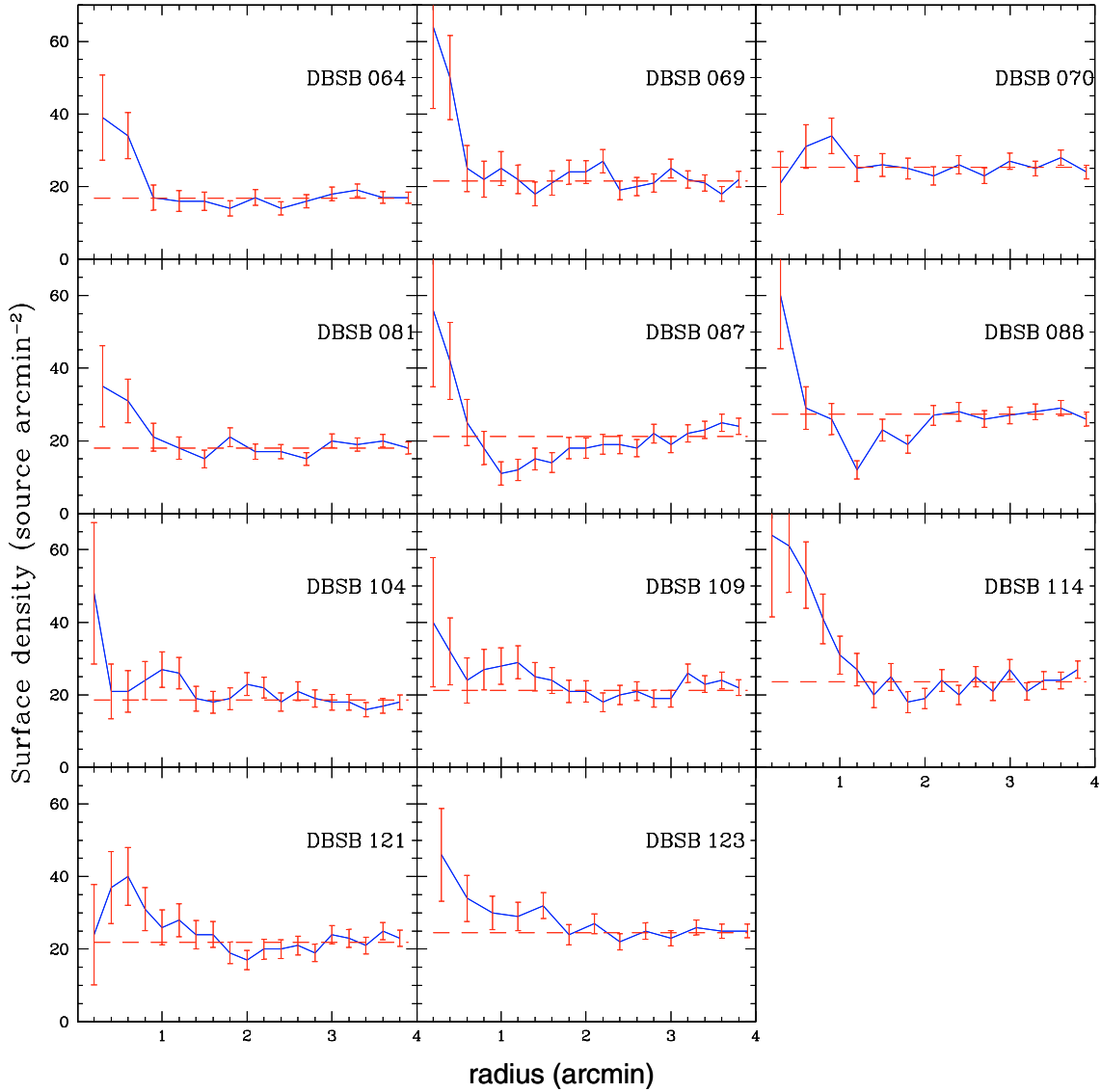
Fig. 6. Same as in Fig. 5 for the remaining objects.

method the essential information is given by those stars which present K_s excess and by the total number of cluster members. The K_s fractions for each cluster are given in Table 1.

An estimate of the age for each cluster with known distance was obtained by means of a second method, which involves PMS evolutionary tracks and isochrones of D'Antona & Mazzitelli (1997, 1998). The evolutionary tracks range from 0.07 Myr to 100 Myr for PMS stars with masses from 0.17 $M_\odot$ to 3 $M_\odot$. We adopted a deuterium abundance of 2×10^{-5} and a metallicity of $Z = 0.02$. We converted the theoretical plane into the observational one by using the bolometric corrections of Schmidt-Kaler (1982). For PMS stars younger than 0.3 Myr, we adopted this lower limit age. The age fitting was applied to probable member stars which were individually corrected for absorption (Sect. 4).

5. Analysis

5.1. Individual stars

Spectroscopic data were obtained for 10 out of the 22 clusters. The brightest stars in each cluster were observed. Table 2 shows

Table 2. Positions and spectroscopic results for the brightest stars in the nebulae direction.

Star	α(J2000)	δ(J2000)	J[mag]	ST	A_V
DBSB031_1	08 52 29	−48 46 12	11.681	B34V	2.79
DBSB039_1	09 24 24	−53 07 59	11.909	A7V	0.96
DBSB039_2	09 24 25	−53 08 01	12.727	A57V	1.11
DBSB042_1	10 07 30	−57 32 59	7.424	A89IV	1.35
DBSB049_1	10 51 06	−54 20 42	9.574	A57V	0.60
DBSB049_2	10 51 09	−54 20 25	12.747	B0V	1.44
DBSB049_3	10 51 06	−54 20 51	12.554	B6V	1.35
DBSB069_1	11 33 54	−63 16 38	10.437	B5V	1.56
DBSB069_2	11 33 53	−63 16 52	11.358	B34V	0.81
DBSB070_1	11 48 37	−62 17 26	12.316	G9K0V	0.21
DBSB081_1	12 58 40	−66 22 18	11.070	B6V	1.74
DBSB088_1	14 19 37	−61 25 04	11.724	A13V	0.75
DBSB104_1	17 04 01	−51 05 01	8.163	B34V	0.30
DBSB104_2	17 03 59	−51 04 57	8.550	B34V	0.45
DBSB109_1	16 47 10	−41 16 31	9.526	B12V	1.17

coordinates, J-magnitudes, spectral types and the resulting extinction values A_V.
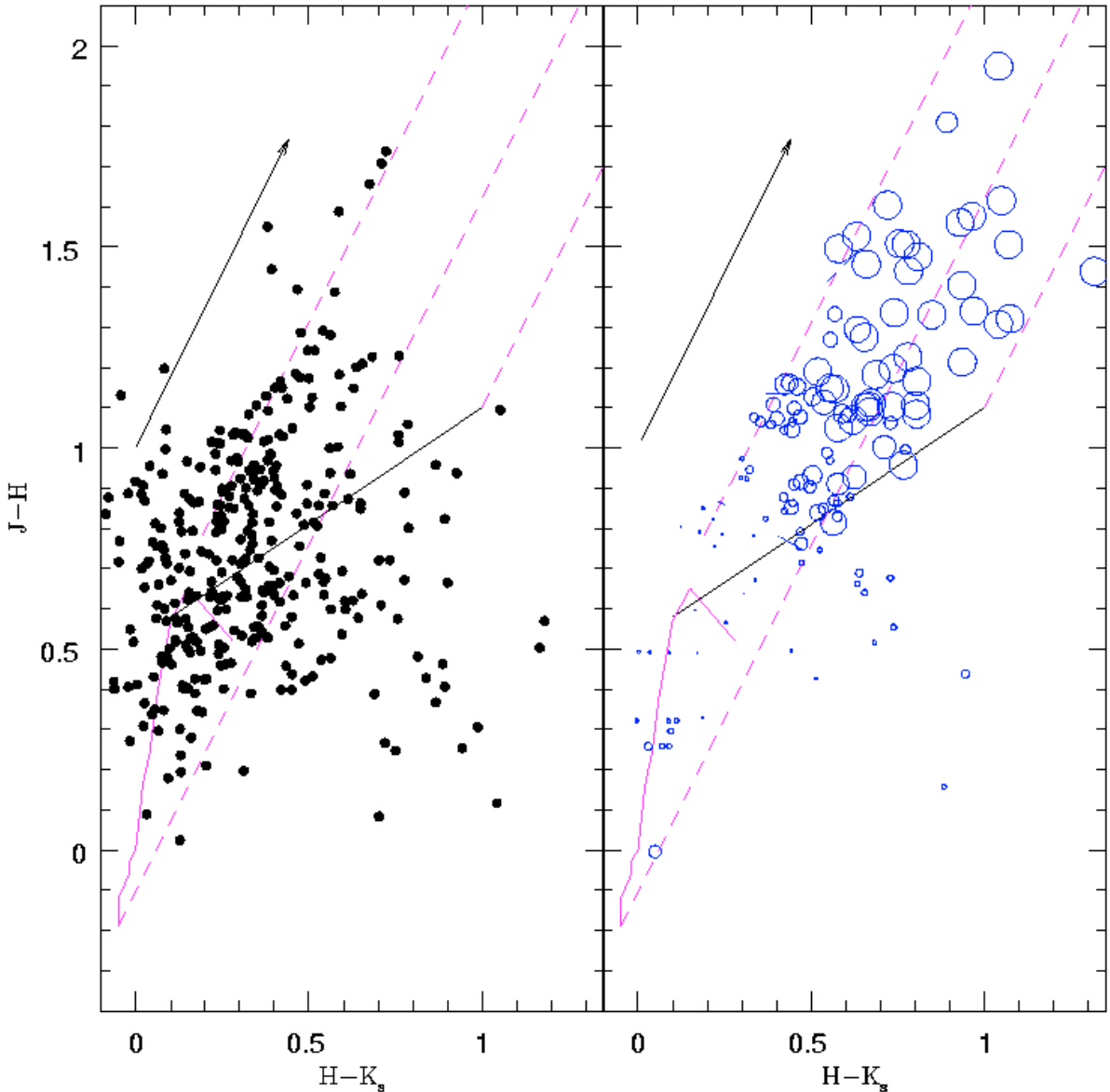
Fig. 7. Illustration of the statistical field star subtraction on the 2CD of DBSB 011. *The left and right panels* show on- and off-cluster stars respectively. Symbol sizes are proportional to the P_{jon} membership probabilities. Reference lines as in Fig. 8.

The bright stars DBSB 042_1, DBSB 049_1 and DBSB 070_1 appear to be foreground stars, all of which affected by low extinction. The earlier spectral type and the absorption obtained for the other stars suggest that they are members of their associated cluster.

The distance moduli for these stars imply distances compatible with the values found for the related nebulae in the literature (Table 1). In the sample of clusters with available spectroscopic data, the DBSB 049 cluster presents the most massive member, a B0V star, according to the derived spectral type. Therefore, clusters in this sample seem to have been formed without the presence of a massive star earlier than B-type, including those clusters situated in an HII region environment.

The extinction derived from the spectroscopy is low if compared with typical mean extinctions for embedded clusters. However, these clusters exhibit a considerable differential reddening. This fact suggests that the dust column in the direction of the brightest star in the cluster is smaller on average than the

dust columns of the rest of the stars. This is possibly due to stellar winds.

5.2. Structure

The relation between source surface density and angular radial distance for the clusters is shown in Figs. 5 and 6. The vertical bars are Poissonian errors. The dashed line indicates the mean star field density, which is obtained by means of the stars contained in the outermost rings (radii from 2′ to 4′). The clusters DBSB 11, DBSB 14, DBSB 31, DBSB 42, DBSB 49, DBSB 64, DBSB 70, DBSB 81, DBSB 88 and DBSB 123 are shown in Figs. 5 and 6, with increased radial bin size (0.3′), to get a more reliable profile. The surface density profile (SDP) of sources presents a significant contrast for most of the star clusters in the sample, when it is compared with the SDP of the background.
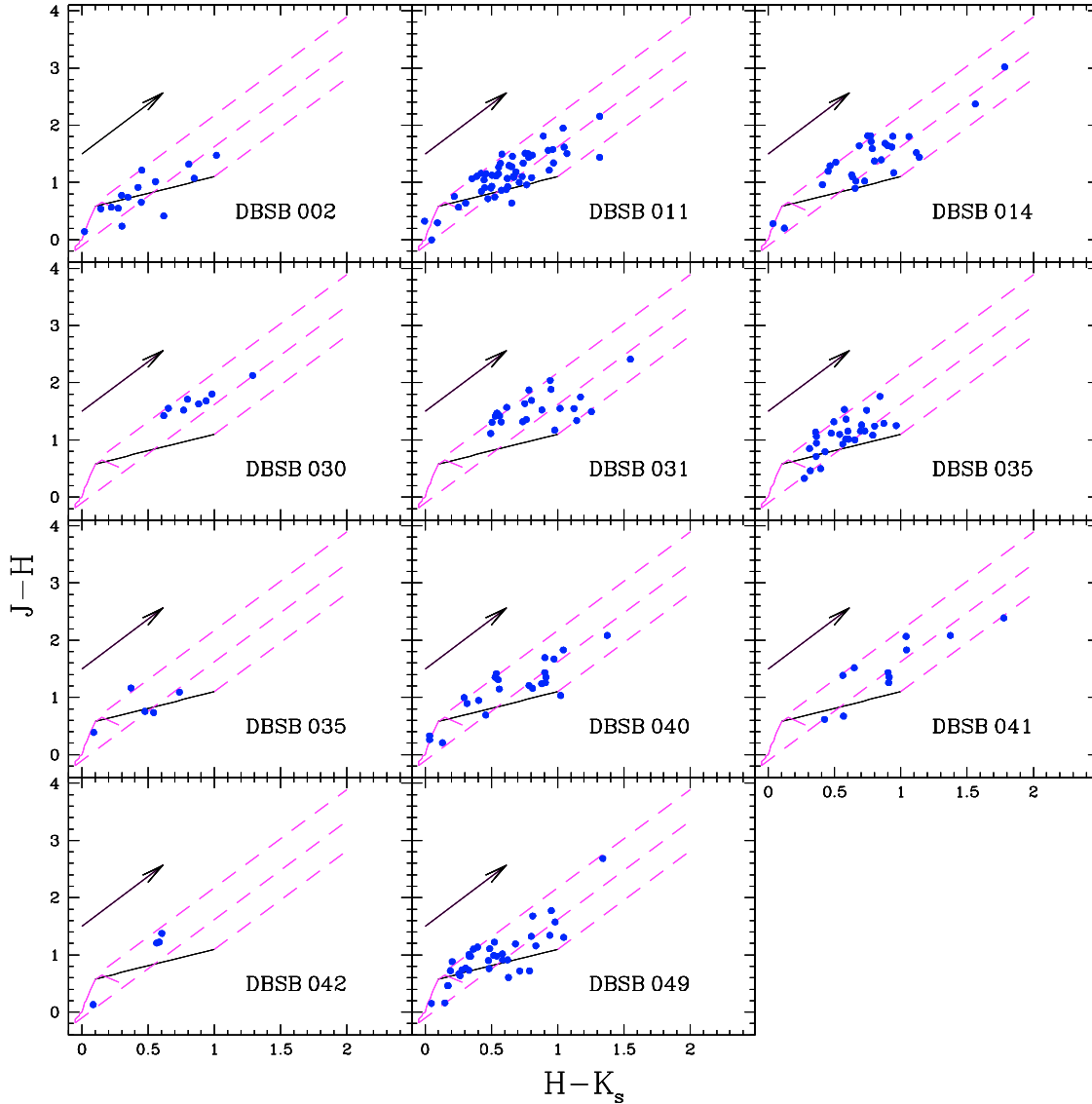
Fig. 8. $((J - H), (H - K_s))$ diagrams. The continuous curve represents the intrinsic distribution of spectral types and the continuous straight line represents the unreddened locus of T Tauri stars. The reddening vector indicates $A_V = 5$. Reddening lines for M 5 giants, O3 stars and T Tauri stars are shown as dashed lines. Faint sources with prohibitive errors were excluded. Each diagram is a realization of the statistical subtraction.

As expected, the larger the Ic index, the larger the contrast between star cluster and its surrounding stellar field in a SDP. For example, the DBSB 114 cluster turned out to have $Ic = 65$, according to its SDP (Table 1).

The angular radius is defined as the limiting radius for the cluster, where the SDP of the object becomes indistiguishable from its surrounding stellar field. The angular radii derived for the sample are in the range of 0.6′ to 2.0′ (Table 1), corresponding to a linear radius in the range of 0.3 to 0.7 pc for the clusters with known distances.

In the 2CD analysis, it is fundamental to decontaminate the clusters for field stars. The points shown in the diagrams are the probable members resulting from a statistical realisation for each cluster. In Fig. 7 we present the 2CD for DBSB 011, to illustrate the method. The left panel shows the surrounding field stars (off-cluster) and the right panel shows the assumed cluster area (on-cluster), with a symbol size proportional to P_{jon}.

Figures 8 and 9 display the decontaminated $((J - H), (H - K_s))$ diagram, which shows intrinsic colours of main

sequence (MS) stars from O3 to M5 (see Binney & Merrifield 1998, and references therein). Reddening lines with a slope $E(J - H)/E(H - K_s) = 1.72$ (Schlegel et al. 1998) for an O3 MS star and an M5 giant, as well as the locus of unreddened T Tauri stars (Meyer et al. 1997) are indicated.

The source distribution along the 2CD is typical of embedded clusters for most objects in the sample, i.e., an important reddening is observed and sources can be seen in the diagram region which T Tauri and AeBe stars occupy.

The number of members derived from the statistical method for each cluster was compared to its Ic index. The correlation coefficient is $r = 0.96$. About 40% of the sources are not detected in all three bands and were not considered in the 2CD analysis, although they were included in the Ic index calculation. Therefore, this index points to a larger number of members than those obtained from the 2CD analysis.

Only a few probable members in the decontaminated 2CD can be found in objects DBSB 030, DBSB 039, DBSB 042,
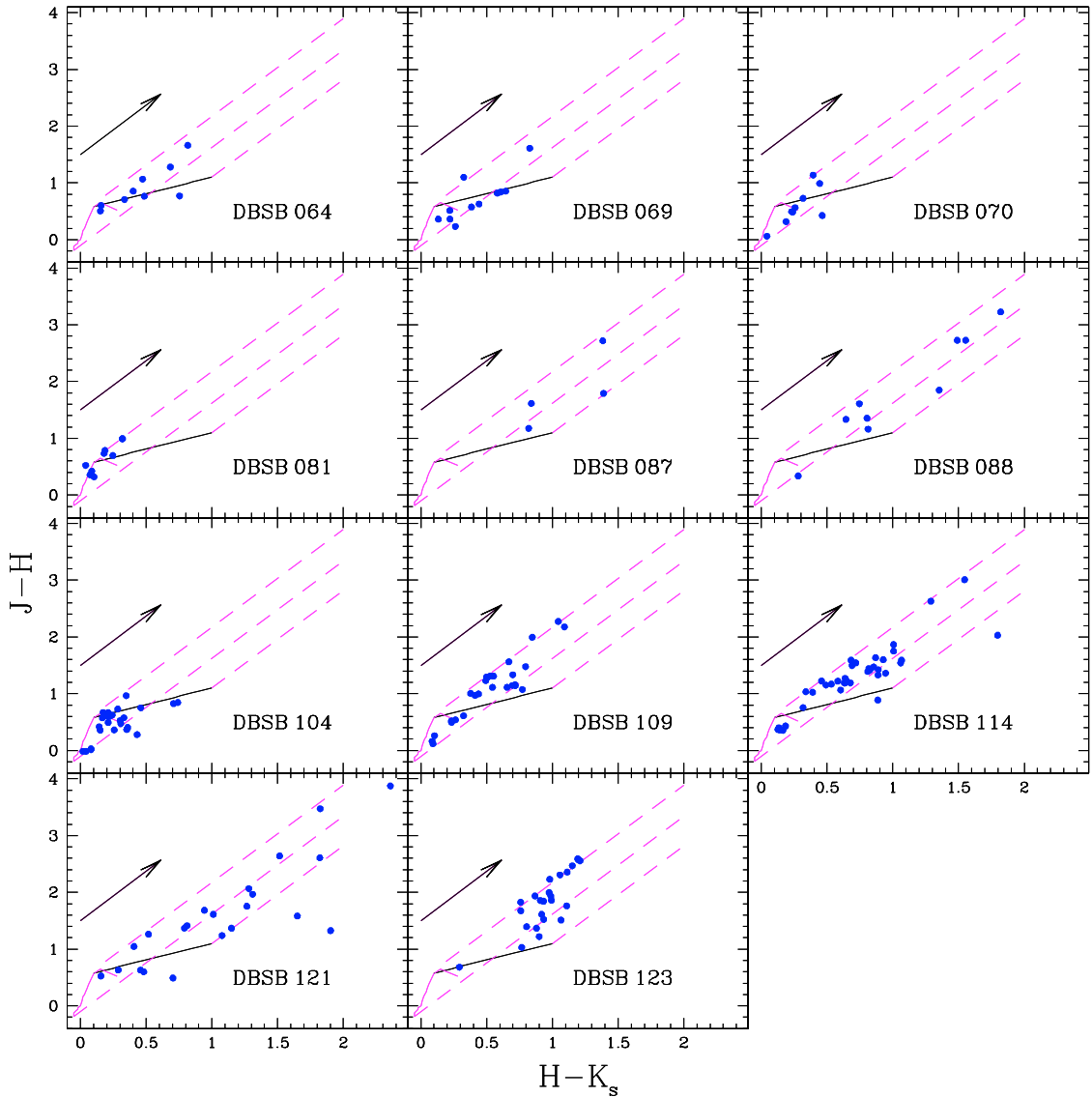
Fig. 9. $((J - H), (H - K_s))$ diagrams for the remaining objects. Symbols as in Fig. 8.

DBSB 081 and DBSB 087. These results, however, are not statistically significant so that deeper observations are recommended.

Interstellar extinction of the stars located in the domain of normal reddening in the $((J - H), (H - K_s))$ diagram, containing weak T Tauri stars, and in the domain of classical K_s values can be obtained by using reddening vectors and intrinsic colours (Soares et al. 2005).

The A_J mean absorption for the clusters in Table 1 indicates that they are not deeply embedded. The extinction values for the stars with available spectroscopy is lower than the mean value of their respective clusters, owing to differential reddening.

Figure 10 shows the K_s excess fraction histogram of the embedded clusters in the sample, except for the low statistic clusters above. Most of the clusters present a K_s excess fraction in the range 0.1−0.3 (Table 1), and none exhibits more than 50% of stars with a K_s excess in the sample. Typical errors in K_s fractions are 0.05.

By means of the percentage of K_s excess stars, one can estimate the age of the cluster or stellar group. Most of the clusters present about 20% of the PMS stars with infrared excess, which suggests an evolutionary stage similar to that of the IC 348 cluster which is 2−3 Myr old (Haisch et al. 2001). In the sample,

Table 3. Age and age dispersion of the clusters based on PMS fits.

Cluster	Age (Myr)	Age dispersion (Myr)
DBSB 031	0.9 ± 0.3	1.6 ± 0.7
DBSB 049	2.1 ± 0.3	2.9 ± 0.4
DBSB 069	3.0 ± 1.1	3.1 ± 1.7
DBSB 088	1.2 ± 0.5	1.6 ± 0.9
DBSB 104	6.0 ± 0.9	3.5 ± 0.4
DBSB 109	1.1 ± 0.4	2.0 ± 0.8

5 clusters have a K_s excess fraction larger than 40%, as is the case of the Taurus dark clouds, which have an estimated age of about 1−2 Myr (Kenyon & Hartmann 1995).

The age determination from the PMS isochrone fit was applied only to the clusters with known distance. Table 3 shows the age and age dispersion for each cluster obtained from the statistical realisations, together with their respective errors.

There may be residual field contamination in the cluster 2CDs. The age dispersions are not only non-negligible but also compatible with the expected dispersions for the cluster formation stage. The dispersions were obtained from the values
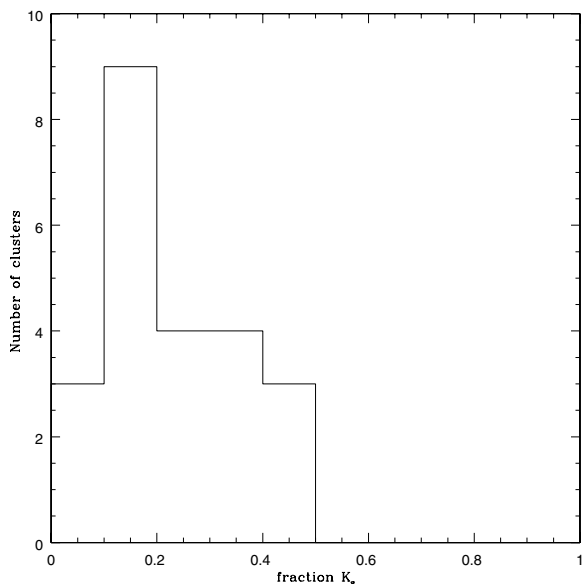
Fig. 10. K_s-excess fraction histogram of the clusters in the sample with good statistics.

found from several realisations of the statistical subtraction (Sect. 4). The error presented in Table 3 does not include the reddening and distance estimation uncertainties. It is probable that due to these errors, there is not a precise correlation between the K_s fraction and the age derived from the PMS method (Table 3).

The total mass estimated for each cluster with known distance was obtained assuming a universal IMF (Sect. 4). We used isochrones of 1 and 2 Myr, according to the evolutionary PMS stage of each cluster in this sample. The derived total mass for most clusters turned out to be lower than $M_T = 100\ M_\odot$ (Table 1).

The masses estimated for the clusters in the sample indicate them to be unbounded stellar systems (Kroupa & Boily 2002)

6. Concluding remarks

A sample of 22 candidate embedded stellar systems in reflection nebulae and/or HII environments were investigated by means of optical spectroscopy and near infrared photometry. Our analysis was based on source surface density and 2CDs, using 2MASS data together with theoretical PMS isochrones.

These stellar systems appear to be low mass embedded stellar clusters containing few stars. Their A_J absorptions and ages point to an evolutionary stage similar to that of the clusters in the reflection nebulae studied in Soares et al. (2005).

In the sample of clusters with the available spectroscopic data gathered at CASLEO, DBSD 049 contains the most massive member, a B0V star. Therefore, the clusters in this sample including those in an HII environment, were formed without the presence of a massive star earlier than B-type.

The total mass estimated for each cluster with known distance was obtained assuming a universal IMF. The derived total mass for most clusters turned out to be lower than $M_T = 100\ M_\odot$.

This fact indicates that they are unbound stellar systems according to Kroupa & Boily (2002). Apparently, embedded low mass clusters have been supplying stars to the Galactic field for generations (Soares et al. 2005).

References

Ahumada, A. V., Clariá, J. J., Bica, E., & Piatti, A. E. 2000, A&A, 141, 79
Ahumada, A. V., Clariá, J. J., Bica, E., Dutra, C. M., & Torres, M. C. 2001, A&A, 377, 845
Bica, E., Dutra, C. M., & Barbuy, B. 2003a, A&A, 397, 177
Bica, E., Dutra, C. M., Soares, J., & Barbuy, B. 2003b, A&A, 404, 223
Binney, J., & Merrifield, M. 1998, Galactic Astronomy, ed. J. P. Ostriker, & D. N. Spergel, Princeton, 107
Brand, J., Blitz, L., & Wouterloot, J. G. A. 1986, A&AS, 65, 537
Caswell, J. L., & Haynes, R. F. 1987, A&A, 171, 261
Carpenter, J. M., Snell, R. L., Schloerb, F. P., & Skrutskie, M. F. 1993, ApJ, 407, 657
D'Antona, F., & Mazzitelli, I. 1997, Evolution of low mass stars in cool stars in Clusters and Associations, ed. G. Micela, & R. Pallavicini, Mem. S. A. It., 68, 807
D'Antona, F., & Mazzitelli, I. 1998, A role for superadiabatic convection in low mass structures, in Brown Dwarfs and Extrasolar Planets, ed. R. Rebolo, E. Martin, & M. R. Zapatero Osorio, ASP Conf. Ser., 442
Dutra, C. M., Bica, E., Soares, J., & Barbuy, B. 2003, A&A, 400, 533
Gum, C. S. 1955, Mem. RAS, 67, 15
Haisch, K. E., Jr., Lada, E. A., & Lada, C. J. 2001, AJ, 121, 2065
Ivanov, V. D., Borissova, J., Pessev, P., Ivanov, G. R., & Kurtev, R. 2002, A&A, 394, L1
Kenyon, S. J., & Hartmann, L. 1995, ApJS, 101, 117
Kroupa, P., & Boily, C. M. 2002, MNRAS, 336, 1188
Kuchar, T. A., & Clark, F. 1997, ApJ, 488, 224
Lada, C. J., & Adams, F. 1992, ApJ, 393, 278
Lada, C. J., & Lada, E. A. 2003, ARA&A, 41, 115
Lauberts, A. 1982, ESO/Uppsala survey of the ESO(B) atlas, Garching: ESO
Mercer, E. P., Clemens, D. P., Meade, M. R., et al. 2005, ApJ, 635, 560
Meyer, R. M., Calvet, N., & Hillenbrand, L. A. 1997, AJ, 114, 288
Muench, A. A., Lada, E. A., Lada, C. J., & Alves, J. 2002, ApJ, 573, 366
Rodgers, A. W., Campbell, C. T., & Whiteoak, J. B. 1960, MNRAS, 121, 103
Schlegel, D. J., Finkbeiner, D. P., & Davis, M. 1998, ApJ, 500, 525
Schmidt-Kaler, T. 1982, in Landolt-Börnstein, New Series, Group VI, Vol. 2b (Springer-Verlag, Berlin), 1
Silva, D. R., & Cornell, M. E. 1992, ApJS, 81, 865
Skrutskie, M., Schneider, S. E., Stiening, R., et al. 2006, AJ, 131, 1163
Soares, J. B. 2006, Estágios iniciais de aglomerados estelares, Ph.D. Thesis, UFRGS, Porto Alegre, Brazil
Soares, J. B., & Bica, E. 2002, A&A, 388, 172
Soares, J. B., & Bica, E. 2003, A&A, 404, 217
Soares, J. B., Bica, E., Ahumada, A. V., & Clariá, J. J. 2005, A&A, 430, 987
Stone, R. P. S., & Baldwin, J. A. 1983, MNRAS, 204, 347
Testi, L., Palla, F., & Natta, A. 1998, A&AS, 133, 81